# Hydrogen Balmer Emission Lines and the Complex Broad Line Region Structure

G. La Mura[*,a], F. Di Mille[a], L. Č. Popović[b,c], S. Ciroi[a], P. Rafanelli[a], D. Ilić[d]

[a]*Department of Astronomy, University of Padova, Vicolo dell'Osservatorio 3, I-35122 Padova, Italy*
[b]*Astronomical Observatory, Volgina 7, 11060 Belgrade, Serbia*
[c]*Isaac Newton Institute of Chile, Yugoslavia Branch, 11060 Belgrade, Serbia*
[d]*Department of Astronomy, Faculty of Mathematics, University of Belgrade, Studentski trg 16, 11000 Belgrade, Serbia*



**Abstract**

In this work we investigate the properties of the broad emission line components in the Balmer series of a sample of Type 1 Active Galactic Nuclei (AGN). Using the Boltzmann Plot method as a diagnostic tool for physical conditions in the plasma, we detect a relationship among the kinematical and thermo-dynamical properties of these objects. In order to further clarify the influence of the central engines on the surrounding material, we look for signatures of structure in the broad line emitting regions, that could affect the optical domain of the observed spectra. Using a combination of line profile analysis and kinematical modeling of the emitting plasma, we study how the emission line broadening functions are influenced by different structural configurations. The observed profiles are consistent with flattened structures seen at quite low inclinations, typically with $i < 20°$. Since this result is in good agreement with some independent observations at radio frequencies, we apply a new formalism to study the properties of AGN central engines.

*Key words:* galaxies: active, galaxies: nuclei, galaxies: Seyfert, line: profiles, quasars: emission lines

## 1. Introduction

The spectrum of a Type 1 AGN is characterized by the presence of prominent broad emission lines, with a full width at half the maximum (FWHM) which corresponds to velocity fields exceeding $10^3\,\mathrm{km\,s^{-1}}$. The properties of the emission lines are connected to the physical conditions within the source and they suggest that the lines are mainly originated by electron - ion recombinations in a photo-ionized plasma (see e. g. Osterbrock , 1989). Unfortunately, since the broad components of these spectral features are originated very close to the center of the source, the structure of the so called Broad Line Region (BLR) cannot be spatially resolved by our observations. This limit affects our ability to investigate the physics of AGN and to provide a self-consistent theoretical interpretation of their observational properties.

At present it is widely accepted that AGN are powered by matter accreting into the gravitational field of a *Super Massive Black Hole* (SMBH), since the gravitational binding energy of the accretion flow may provide the ionizing radiation field, required to drive the observed line emission from the surrounding plasma. Assuming the BLR to be in virial equilibrium under the dynamical influence of this central engine (see, for instance, Peterson & Wandel , 1999; Woo & Urry , 2002; Sulentic et al. , 2006, etc.) the mass of the black hole might be estimated with an expression in the form of:

$$M_{\mathrm{BH}} = f \cdot \frac{R_{\mathrm{BLR}}\,\Delta v^2}{G}, \qquad (1)$$

where $G$ is the gravitational constant, $R_{\mathrm{BLR}}$ an estimate of the BLR extension, and $\Delta v$ a measurement of the gas radial velocity distribution. The factor $f$ accounts for the unknown structure of the gas motion pattern. It is required in order to estimate the actual kinematical properties from the line of sight velocity distribution, that we measure in the spectra, and it is therefore referred to as the *geometrical factor*.

Many works deal with the relationship among the emission line profiles and the actual dynamics of the BLR (see, for instance, Capriotti et al. , 1980, 1981; Netzer , 1990; Ferland et al. , 1992). Recent investigations, such as those of Vestergaard et al. (2000) and Nikołajuk et al. (2005), point towards a considerably flattened geometry, which is consistent with the existence of an accretion disk around the SMBH. In this progress report, we describe the analysis which we performed on a sample of Type 1 AGN spectra, in order to examine the influence of the AGN central engines onto the surrounding BLR plasma. With a combination of observations, analytical calculations and theoretical models, we look for indications of the BLR structural properties in the emission line profiles. We organize this report as follows: in §2 we introduce the relation among BLR kinematical and thermo-dynamical properties; in §3 we outline the analytical formalism, that we exploit to

*Corresponding author (phone number +39 3391845700)
*Email addresses:* giovanni.lamura@unipd.it (G. La Mura), francesco.dimille@unipd.it (F. Di Mille), lpopovic@aob.bg.ac.yu (L. Č. Popović), stefano.ciroi@unipd.it (S. Ciroi), piero.rafanelli@unipd.it (P. Rafanelli), dilic@matf.bg.ac.yu (D. Ilić)

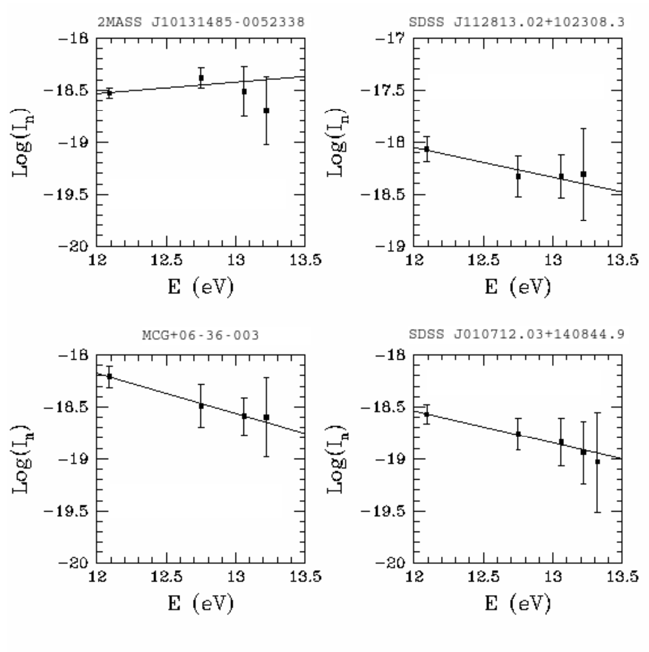


Figure 1: Four examples of Boltzmann Plots applied to the spectra of the BLR in some Type 1 AGN: in the upper left panel no straight line fit is achieved (class iv); in the upper right panel only a poor fit, with a relative uncertainty $\Delta A/A > 0.2$ in the temperature parameter, is performed (class iii); the bottom left panel gives a good fit, but H$\epsilon$ could not be detected in the spectrum (class ii); finally the bottom right panel shows a straight line fit to the normalized intensities of the Balmer series up to H$\epsilon$ (class i).

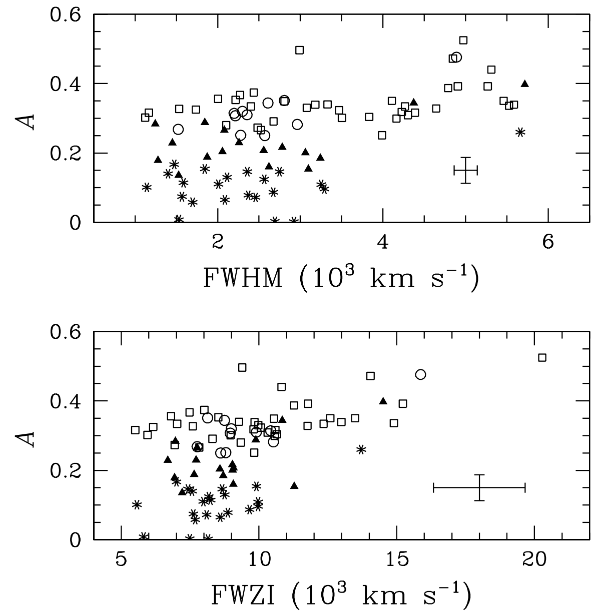


Figure 2: $A$ parameter as a function of the BLR velocity fields, inferred by both the FWHM and FWZI of the Balmer lines: the open circles are sources of class i; the open squares represent objects of class ii; filled triangles are spectra of class iii and, finally, asterisks are objects with BP class iv. The crosses in the lower right corners of each panel are the median uncertainties of measurements.

investigate the BLR structure; in §4 we discuss the predictions of our BLR structural models; finally §5 is devoted to the discussion of the results achieved by comparing models and observations, with a mention to some possible tests and to the implications related to the use of spectroscopic measurements in our sample of AGN.

## 2. Plasma physics with the Boltzmann Plots

Due to its high density and strong interactions with the ionizing radiation field, the BLR plasma cannot be studied by means of the standard spectroscopic techniques, that are commonly adopted in other low density nebular environments. This characteristic forces us to adopt alternative techniques to investigate its properties. Looking at the flux in the broad component of an emission line, it is possible to introduce a *normalized line intensity*, with respect to the atomic constants which characterize the corresponding transition, in the form of:

$$I_{\rm n} = \frac{\lambda_{ul}\, F_{ul}}{g_u\, A_{ul}}, \tag{2}$$

where $\lambda_{ul}$ is the line wavelength for a transition from an upper level $u$ to a lower level $l$, $F_{ul}$ is the observed flux, $A_{ul}$ the spontaneous transition probability, and $g_u$ the upper level's statistical weight. Looking at the normalized emission line intensities of some spectral features, belonging to the same transition series, it can be shown that if the plasma approaches a condition of Local Thermo-dynamical Equilibrium (LTE), we get (Popović , 2003, 2006):

$$\log I_{\rm n} = B - A\, E_u, \tag{3}$$

where $E_u$ represents the upper level's excitation energy for the transition, $B$ is a constant for all the emission lines in the series, while $A$ takes the role of a *temperature parameter*, corresponding to:

$$A = \log e/(k_{\rm B} T_e), \tag{4}$$

with $k_{\rm B}$ representing the Boltzmann constant and $T_e$ an average value of the electron temperature in the plasma.

The diagrams which show the emission line normalized intensities of the Balmer series as a function of the upper level's excitation energies are known as Boltzmann Plots (BP). A strict interpretation of the BP results, however, requires that the physical conditions in the line emitting region should not change abruptly. Otherwise the simple formulation of the emission line intensities in the series would not be possible and the LTE approximation would subsequently fail. In Fig. 1 we give some examples, showing four different situations, that we commonly observe, applying the BP to the BLR plasma of some AGN (La Mura et al. , 2007). Extracting the BLR signal from our spectra, we computed the emission line normalized intensities of the Balmer series as in Eq. (2). We performed

several flux measurements, that were subsequently averaged together and compared with the spectral noise fluctuations, in order to estimate the mean values and their uncertainties, therefore assuming the error of the BP to be given by:

$$\Delta(\log I_{\rm n}) = \frac{3\,\sigma_{Ful}}{F_{ul}}, \tag{5}$$

with $\sigma_{Ful}$ representing the emission line flux dispersion. Repeating the emission line flux estimates was a fundamental step, because of the large difficulties associated with flux measurements in the broad line components, in a spectral region where several contributions to the observed emission are blended together.

The temperature parameters extracted from our BP and illustrated in Fig. 2 appear to be related to the emission line profiles, in the sense that higher values of $A$ and better realizations of the prediction of Eq. (3), are commonly found in the range of broad line emitting objects. Unfortunately our sample is not particularly representative in this region, but the circumstance suggests that the thermo-dynamical properties of sources with various emission line widths are under the influence of different ionizing radiation fields, as it would be expected when powering the central engines of these AGN with different combinations of SMBH mass and accretion rate. In order to improve our understanding of the role played by these fundamental parameters, we further investigated the processes which lead to the formation of the observed line profiles and their relations with the actual source's dynamical properties.

## 3. Balmer emission line profile analysis

### *3.1. Emission line broadening from cross-correlation*

The BLR spectrum shows several emission lines corresponding to many permitted and some semi-forbidden transitions of variously ionized atomic species. In the optical domain, the Balmer series of hydrogen provides a set of bright emission lines belonging to a well defined family of interactions among matter and radiation, whose profiles are influenced by the kinematics of gas.

To perform our study, we adopted the cross-correlation formalism, originally described by Tonry & Davis (1979) and then updated by Statler (1995). As a starting point, we can approximate the spectrum of a broad line emitting source as the convolution of an appropriate template of narrow emission lines $T(x)$ with the corresponding broadening function $B(x)$:

$$S(x) \simeq T(x) * B(x), \tag{6}$$

where $S(x)$ is the observed spectrum, while $x$ represents a logarithmic wavelength coordinate of the form $x = A\ln\lambda + B$, such that the effect of radial velocities results in linear shifts along $x$. Introducing the cross-correlation function of the spectrum with the template:

$$X(x) = S(x) \otimes T(x) = \int S(x)T(x+x')\,{\rm d}x', \tag{7}$$

it can be shown that the cross-correlation function (XCF) approximates the convolution among the template's auto-correlation function (ACF) and the kinematical broadening function (BF) of the object (Statler , 1995; La Mura et al. , 2009):

$$X(x) \simeq [T(x) \otimes T(x)] * B(x). \tag{8}$$

Since $T(x)$ is known and $X(x)$ is drawn from observations, as far as the template is correct, it is possible to recover $B(x)$.

Restricting our analysis to the primary cross-correlation peak, which carries most of the kinematical information and it is weakly affected by template mismatch, Eq. (8) has a discrete form that, using the simplified notation $F_i = F(x_i)$, becomes:

$$X_k \simeq \sum_{i=0}^{N}\left(\sum_{j=0}^{N} T_i\,T_{i+j}\right) B_{k-i}. \tag{9}$$

Provided that all the functions are null when they are computed outside the range $0 \le i \le N$, Eq. (9) defines a system of $N+1$ linear equations in the $N+1$ variables $B_{k-i}$ ($k \ge i$). A standard $\chi^2$-minimization routine can be therefore used to solve the problem.

### *3.2. Analytical expressions for the broadening functions*

The BLR emission lines are influenced by the effects of complex kinematics within the source and of radiation transfer from the source to the observer. For this reason it is hardly conceivable that a simple analytic expression might be used to fit the resulting profiles. In the simple case of a random motion distribution, the emission line profiles would approximately match a Gaussian function, but, in presence of ordered kinematical components, we expect significant deviations from this shape. A good way to estimate the importance of such various effects is to parameterize the observed BF by means of a Gauss-Hermite orthonormal expansion, similarly to what is described in Van Der Marel & Franx (1993) for the case of stellar kinematics in elliptical galaxies. Following their method, if we call $\alpha(v)$ the normal Gaussian function:

$$\alpha(v) = \frac{1}{\sqrt{2\pi}\sigma_v}\exp\left(-\frac{v^2}{2\sigma_v^2}\right), \tag{10}$$

where $\sigma_v$ is the line of sight velocity dispersion, we may express the emission line BF as:

$$B(v) = B_0\alpha(v - V_{sys})\left[1 + \sum_{i=3}^{N} h_i H_i(v - V_{sys})\right], \tag{11}$$

where we call $B_0$ the BF normalization factor, $V_{sys}$ the systemic radial velocity offset between the BF and the chosen reference frame, $H_i(v - V_{sys})$ the $i^{\rm th}$ order Hermite polynomial, and $h_i$ the corresponding coefficient. A wide description of the properties of the Hermite polynomials is given in Van Der Marel & Franx (1993). It is

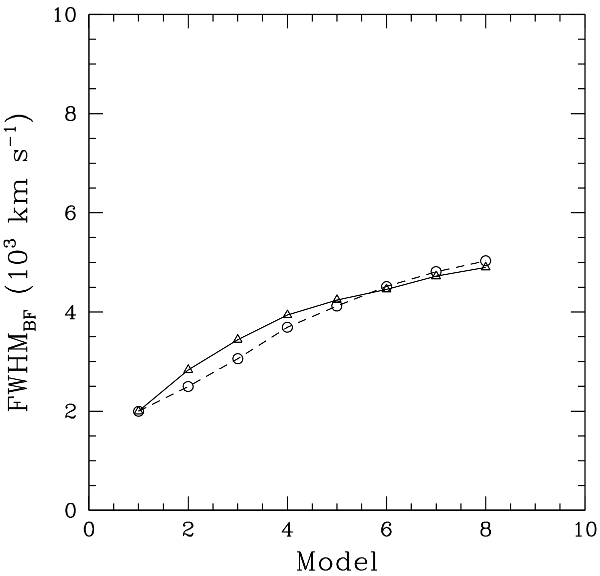


Figure 3: Mass - inclination degeneracy. In this plot we illustrate the expected FWHM in the BF of emission lines originated in a disk structure. The empty triangles connected by the continuous line are the predicted values for reference disk models with $i = 10°$ in the gravitational field of black holes with $M_{BH} = 1$, 2, 4, 6, 8, 10, 12, and 14 $\cdot 10^7 \mathrm{M}_\odot$ (respectively models from 1 to 8); the circles with the dashed line show the predicted behavior for the reference disk model in the gravitational field of the black hole with $M_{BH} = 10^7 \mathrm{M}_\odot$, when seen under inclinations of $i = 10°$, 15°, 20°, 25°, 30°, 35°, 40°, and 45° (again from model 1 to 8).

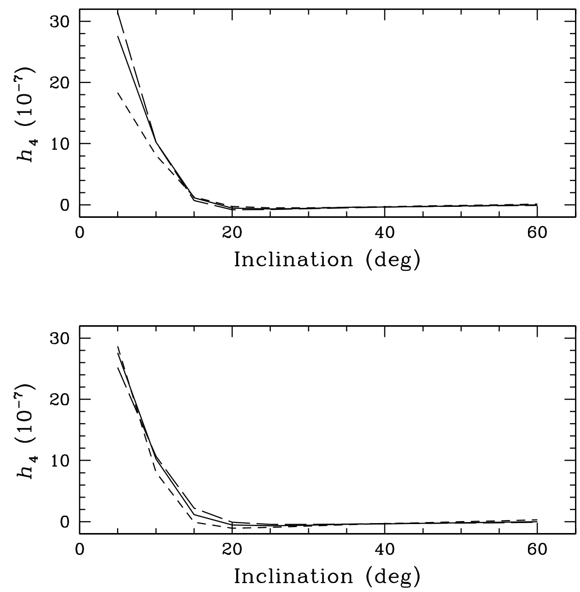


Figure 4: The effect of inclination on the symmetric distortion of the BF. Here we show a comparison of the reference model predictions concerning the BF symmetric component (continuous lines) with four variants: in the upper panel we plot models with stronger (long dashed line) and weaker (short dashed line) disk emission with respect to the surrounding gas distribution; in the bottom panel we show the differences obtained by setting $\sigma_{Bell} = 0.07\,c$ (short dashed line) and $\sigma_{Bell} = 0.09\,c$ (long dashed line).

demonstrated that odd order functions account for asymmetric distortions of the Gaussian profile, while even order functions have a symmetric effect. Truncating Eq. (11) to $N = 4$, the Hermite polynomials are expressed by:

$$H_3(y) = \frac{1}{\sqrt{6}}(2\sqrt{2}y^3 - 3\sqrt{2}y) \qquad (12a)$$

$$H_4(y) = \frac{1}{\sqrt{24}}(4y^4 - 12y^2 + 3). \qquad (12b)$$

Therefore, it is possible to estimate the role of non-Gaussian kinematical components, using the whole BF profile, simply by fitting the observed shape with a truncated Gauss-Hermite series and measuring the appropriate values of $h_3$ and $h_4$.

### *3.3. The Balmer line broadening functions*

Applying our formalism to a set of BLR spectra, collected at the *Sloan Digital Sky Survey* (SDSS) spectroscopic database (see Adelman-McCarthy et al. , 2008; La Mura et al. , 2009, for more discussion), our task is then to recover their BF. To calculate the cross-correlation functions, we build a template of Balmer emission lines, following the median line intensity ratios found by La Mura et al. (2007). The template assumes that the SDSS instrumental profile is a Gaussian function with FWHM = $167\,\mathrm{km\,s^{-1}}$. At the spectral resolution of Sloan data, the logarithmic sampling of the wavelength coordinate can be performed with discrete bins corresponding to 69 $\mathrm{km\,s^{-1}}$ each. We compute the template's ACF:

$$A(x) = T(x) \otimes T(x) \qquad (13)$$

and the cross-correlation functions of the BLR spectra with the template, following the definition of Eq. (7). Applying the least squares formalism to the equation system (9), it follows that the BF of each spectrum must satisfy the relations:

$$\sum_{i=0}^{N} B_i \left( \sum_{j=0}^{N} A_j A_{i-k} \right) = \sum_{i=k}^{N} A_{i-k} X_i. \qquad (14)$$

## 4. BLR kinematical and structural models

Since the BLR structure cannot be represented by a random motion pattern, the shape of the broad emission lines may exhibit large deviations from the Gaussian profile. If the BLR has a flattened component which is seen at low inclination the geometrical structure can considerably affect the dynamical interpretation of spectroscopic

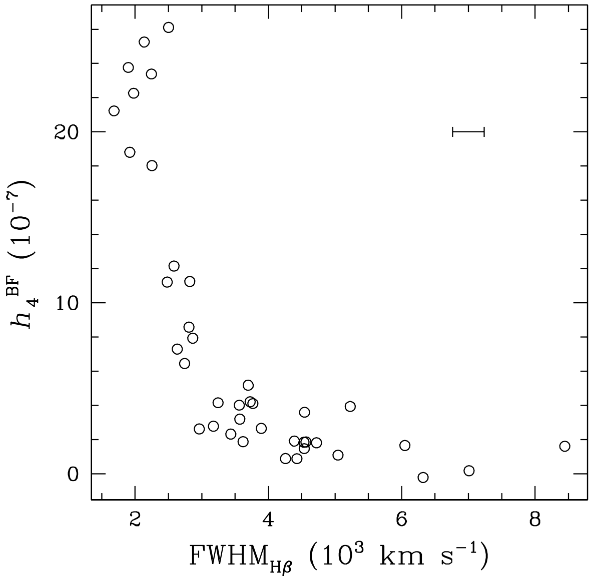


Figure 5: BF symmetric distortion plotted as a function of $\mathrm{FWHM}_{\mathrm{H}\beta}$. We observe a large evolution of the symmetric component as a function of broadening, suggesting the possibility of inclination effects in nearly face-on flattened structures. Such effects become weaker as the profile width increases.

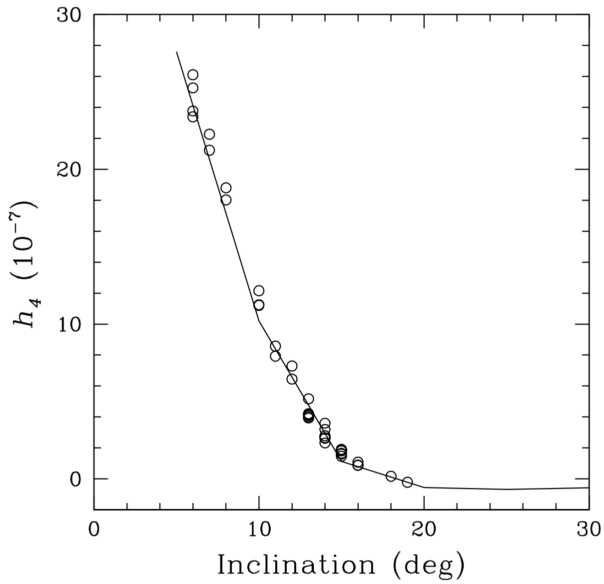


Figure 6: BLR inclination inferred by comparison among the BF symmetric component $h_4$, predicted by the reference model for various inclinations, and the corresponding distribution observed in our data. According to the model predictions, the $h_4$ coefficient is very sensitive to flattening and inclination in nearly face-on structures, while it becomes a weaker indicator for larger inclinations.

data. We illustrate this concept in Fig. 3, where we plot the expected FWHM in the broadening function produced by disks surrounding black holes of increasing mass and we compare it to the situation of a black hole of fixed mass, but with the disk seen under different inclinations.

Exploiting a combined BLR structural model, involving an accretion disk and a surrounding distribution of gas (Chen et al. , 1989; Chen & Halpern , 1989; Popović et al. , 2004), we computed a range of emission line profiles, studying the effect of source inclination. Our reference model assumes $R_{in} = 1834\,R_S$ for inner radius, $R_{BLR} = 18340\,R_S$ for outer radius, $\sigma_{Disk} = 0.003\,c$ as the intrinsic velocity dispersion in the disk, and $\alpha = -2.0$ for the radial emission power law, where $R_S$ and $c$ represent the Schwarzschild radius and the speed of light. Moreover, this model includes a surrounding gas distribution having a velocity dispersion of $\sigma_{Bell} = 0.008\,c$. This model carries out the best match to the observed line profiles with the assumption of various disk inclinations.

In Fig. 4, we compare the reference model with some variants, obtained with slightly different parameters. We note that all the models predict a strong dependence of the symmetric non-Gaussian component (the coefficient $h_4$ in the Gauss-Hermite expansion) on the disk inclination, in the range of small values of $i$. The reason is quite simple, because a nearly face-on disk enhances the low radial velocity peak of the BF, while an edge-on disk is more likely to affect the high velocity wings.

As we show in Fig. 5, where we plot the measured values of $h_4$ as a function of $\mathrm{FWHM}_{\mathrm{H}\beta}$, there is a remarkable evolution of the symmetric components of the line profiles, which decrease in importance for increasing line profile width. Such an effect suggests that a considerable variation of the geometrical factor $f$ might be present and it should be taken into account in order to estimate the actual properties of the SMBH. Using the model predictions, we can exploit the symmetric distortion coefficient to estimate the inclination of the flattened BLR component and to apply a correction to our dynamical interpretation of the observed line profiles.

## 5. Results and discussion

### *5.1. The BLR geometry*

It can be shown that completely neglecting the role played by the BLR geometrical factor may lead to incorrect black hole mass estimates, with uncertainties that, in the worst cases, could span over two orders of magnitude. Using the line profile analysis to estimate the BLR structural properties, we apply a modified scheme to evaluate the black hole mass in Eq. (1), introducing an *equivalent velocity field*, such that $v_{eq} = f\,\Delta v$, defined as:

$$v_{eq} = \frac{1}{2}\left[\frac{\sqrt{3}}{2}\mathrm{FWHM}_{Bell}(\mathrm{H}\beta) + \frac{\mathrm{FWHM}_{Disk}(\mathrm{H}\beta)}{4\sin i}\right]. \quad (15)$$

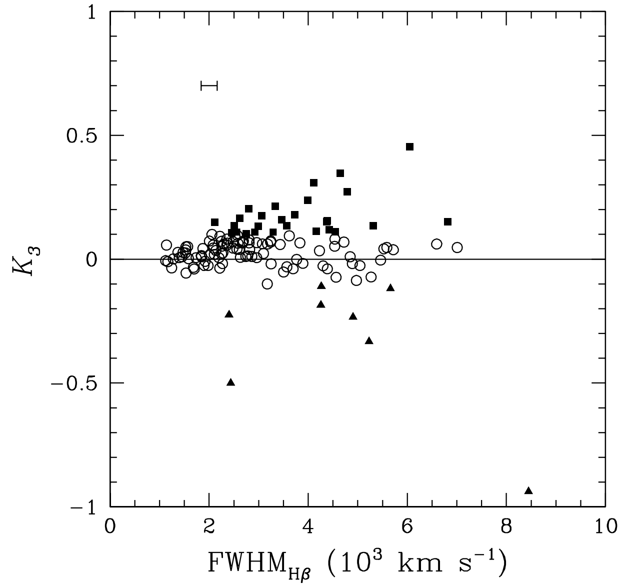


Figure 7: H$\beta$ asymmetry parameter distribution vs. $\mathrm{FWHM}_{\mathrm{H}\beta}$. Filled symbols represent objects where the asymmetric component exceeds 10% of the Gaussian contribution. We plot as triangles objects that are affected by negative asymmetry, yielding red shifted peaks and blue shifted wings, while we use squares to represent positive asymmetry sources, with a blue shifted peak and red shifted wings. Large asymmetries characterize objects where fits with the reference model are more likely to be problematic. The bar in the upper left region of the diagram is a median estimate of the measurement errors.

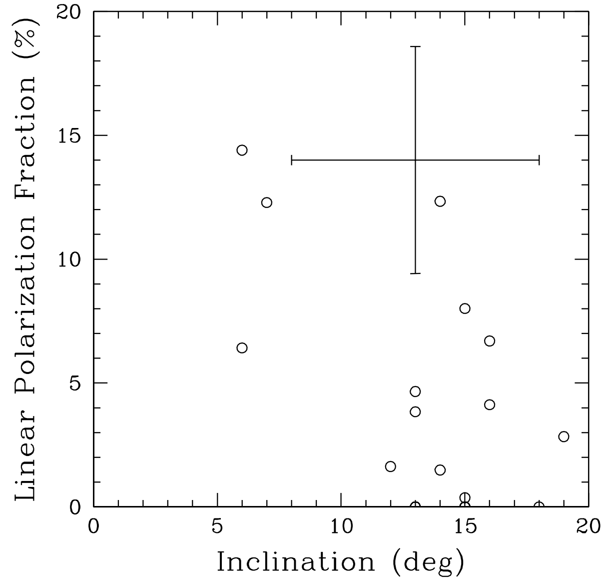


Figure 8: Degree of linear polarization at the radio frequency of 1.4 GHz as a function of the inferred BLR inclination. The cross in the upper left corner gives the median uncertainty estimate. Polarization data are from the NVSS catalogue.

Assuming that the line profile broadening results from both planar and non-planar motions (Labita et al. , 2006; McLure et al. , 2002; Jarvis & McLure , 2006, etc.), $v_{eq}$ combines the velocity estimates obtained from the H$\beta$ emission line profile by fitting two Gaussian functions, which are subsequently compared with the reference model, providing a distinction among the disk and the surrounding gas contributions. The corresponding geometrical factors are assumed to be given by the isotropic interpretation of Netzer (1990) and the projection of a rotating disk, confined in a smaller region with respect to the other component. The inclination of the disk is estimated by comparison of the BF symmetric distortion with that predicted by the reference model, as shown in Fig. 6, while $R_{BLR}$ is inferred by measurements of the optical continuum intensity, according to the empirical relationships found in some recent reverberation mapping campaigns (Kaspi et al. , 2000, 2005; Bentz et al. , 2006).

A particularly important problem, involving the determination of AGN physical properties from emission lines, resides in the line profile asymmetries. Several factors, such as partial obscuration, geometrical structure, or large scale non-virialized motions can produce asymmetric line profiles. Moreover, relativistic effects within the gravitational field of the SMBH give raise to asymmetries, especially in the high velocity wings of the profile, which are included in the calculations of the model by Chen & Halpern (1989). In order to assess how much the asymmetric component affects our estimates of the velocity field, we introduced an asymmetry parameter:

$$K_3 = h_3 H_3(\mathrm{HWHM}_{\mathrm{H}\beta}), \tag{16}$$

expressing the relative contribution of the asymmetric component, with respect to the Gaussian component, in the profile of H$\beta$ at its half-maximum level. As we show in Fig. 7, the asymmetric component gives a contribution to the FWHM which rarely exceeds the 10% level. The most extreme cases, where the asymmetric component becomes larger than 20%, occur only in the range of very broad line emitting sources. Although this property is not particularly well represented in our sample, it echoes the observation of larger asymmetries in objects where $\mathrm{FWHM}_{\mathrm{H}\beta} > 4000\,\mathrm{km\,s^{-1}}$, which is among the features identified by Sulentic et al. (2000, 2006) in their distinction between Population A and B sources. Since there is evidence for different structural configurations in objects with broader and narrower emission lines, at least in the case of radio-loud sources, objects with the largest asymmetries are more problematic in their comparison with the reference model.

*5.2. Implications*

Most of the results achieved in this work depend critically on the choice of our reference model, which leads

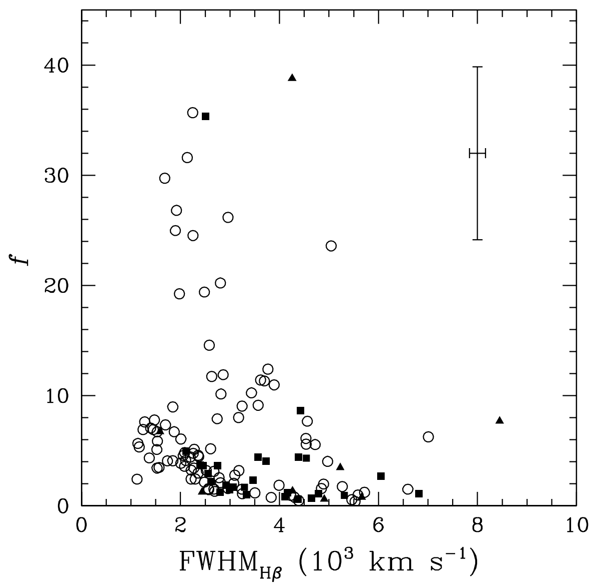


Figure 9: The range of estimated geometrical factors for sources of different FWHM$_{H\beta}$. Open circles represent objects with symmetric profiles, while filled squares and triangles are for sources with positive and negative asymmetries, respectively. The distinction among sources with different degree of asymmetry is required because objects with large asymmetries are harder to compare with the theoretical line profiles, predicted by the reference model.

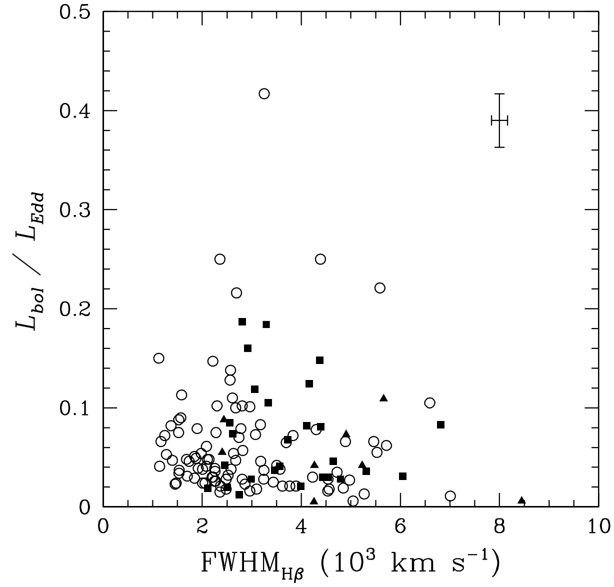


Figure 10: SMBH accretion rates vs. FWHM$_{H\beta}$, using the same symbology as in Fig. 7. The cross in the upper right corner of the diagram is the median uncertainty of measurements. We do not detect either very high accretion rates or systematic trends associated to the line profile widths. Our estimates do not appear to be dramatically affected by the presence of asymmetric profile components.

us to conclude that the BLR has a flattened component, that is commonly seen at $i \leq 20°$. In the case of radio-loud sources, nearly face-on disk structures are likely to produce a radio jet oriented along our line of sight and the resulting signal should be considerably polarized. Indeed, some objects of our sample have been detected in the NRAO VLA Sky Survey (NVSS), which provides measurements of the radio flux and polarization at the frequency of 1.4 GHz (Condon et al. , 1998).[1] We compare the degree of linear polarization with our inclination estimates in Fig. 8. We find that a significant degree of linear polarization is detected in many objects and it appears to be an averagely decreasing function of $i$.

A comparison of our mass determinations with the isotropic assumption allows us to study the properties of the geometrical factor within our sample. The situation depicted in Fig. 9 clearly indicates that significant effects, up to a factor $\sim 40$, should be expected and that they are more commonly observed in the range of sources with FWHM$_{H\beta}$ $\leq 3000 - 4000$km s$^{-1}$. We find that the average value of the geometrical factor for black hole mass determinations based on FWHM$_{H\beta}$ is $f = 6.51$, not very different from the result achieved by Onken et al. (2004), who gave a geometrical factor $f = 5.5 \pm 1.9$ for black hole mass estimates based on the emission line dispersions. We should note, however, that a previous investigation by Collin et al. (2006) applied composite kinematical models to the BLR and compared several estimates of the central engine mass, suggesting a distinction among the geometrical factors needed to correct the velocity fields based on the emission line dispersion and FWHM.

Applying our modified scheme to the calculation of the central engine's dynamical properties, we find that a correction for BLR inclination increases our estimate of the SMBH mass. A direct consequence of this effect is that we do not detect dramatically high accretion rates, with respect to the corresponding Eddington limits. In particular, as it is illustrated in Fig. 10, although we do observe a trend where objects with narrower emission lines have typically higher accretion rates, this property does not appear to hold in the form of a real anti-correlation, as it could look like, when the BLR geometrical properties were not properly considered. Comparing our estimates of accretion rate with the temperature parameters $A$, inferred by means of the BP analysis and plotted in Fig. 11, we find that the occurrence of high accretion rates is generally associated to lower values of $A$ (i. e. higher plasma temperatures), but we detect no particular relationship with the effects that undermine the reliability of the BP method, suggesting that more physical processes should be involved in this problem.

[1]Polarization data are available at the web site http://www.cv.nrao.edu/nvss/NVSSlist.shtml

tory, and the University of Washington.

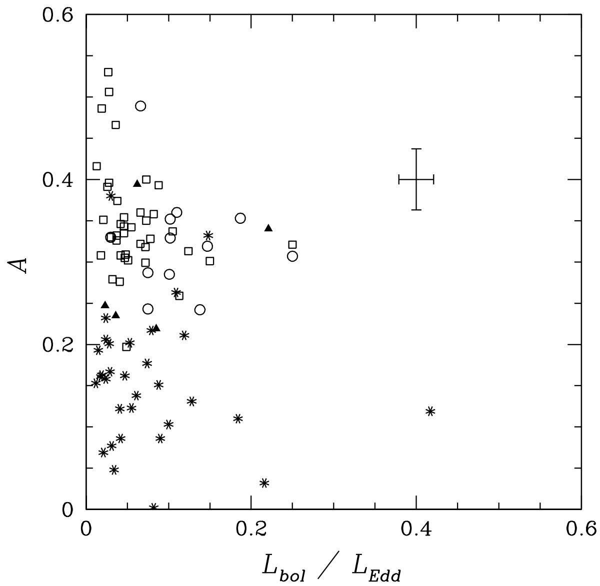


Figure 11: The temperature parameter $A$ compared with the estimated accretion rate, in objects with different BP classification (symbols are the same as in Fig. 2). Lower values of $A$ are observed with increasing Eddington ratios.


Acknowledgements

We thank the referee for useful discussion and suggestions concerning the development of our research.

L. Č. Popović was supported by the Ministry of Science of R. Serbia through project 146002 "Astrophysical Spectroscopy of Extragalactic Objects."

Funding for the SDSS and SDSS-II has been provided by the Alfred P. Sloan Foundation, the Participating Institutions, the National Science Foundation, the U.S. Department of Energy, the National Aeronautics and Space Administration, the Japanese Monbukagakusho, the Max Planck Society, and the Higher Education Funding Council for England. The SDSS Web Site is http://www.sdss.org/.

The SDSS is managed by the Astrophysical Research Consortium for the Participating Institutions. The Participating Institutions are the American Museum of Natural History, Astrophysical Institute Potsdam, University of Basel, University of Cambridge, Case Western Reserve University, University of Chicago, Drexel University, Fermilab, the Institute for Advanced Study, the Japan Participation Group, Johns Hopkins University, the Joint Institute for Nuclear Astrophysics, the Kavli Institute for Particle Astrophysics and Cosmology, the Korean Scientist Group, the Chinese Academy of Sciences (LAMOST), Los Alamos National Laboratory, the Max-Planck-Institute for Astronomy (MPIA), the Max-Planck-Institute for Astrophysics (MPA), New Mexico State University, Ohio State University, University of Pittsburgh, University of Portsmouth, Princeton University, the United States Naval Observatory, and the University of Washington.


## References


Adelman-McCarthy, J. K. Agueros, M. A., Allam. S. S., et al. 2008, ApJS, 175, 297

Bentz, M. C., Peterson, B. M., Pogge, R. W., Vestergaard, M., & Onken, C. A. 2006, ApJ, 644, 133

Capriotti, E., Foltz, C., & Byard, P. 1980, ApJ, 241, 903

Capriotti, E., Foltz, C., & Byard, P. 1981, ApJ, 245, 396

Chen, K. & Halpern, J. P. 1989, ApJ, 344, 115

Chen, K., Halpern, J. P., & Filippenko, A. V. 1989, ApJ, 339, 742

Collin, S.,Kawaguchi, T., Peterson, B. M., & Vestergaard, M. 2006, A&A, 456, 75

Condon, J. J., Cotton, W. D., Greisen, E. W., Yin, Q. F., Perley, R. A., Taylor, G. B., & Broderick, J. J. 1998, AJ, 115, 1693

Ferland, G. J., Peterson, B. M., Horne, K., Welsh, W. F., & Nahar, S. N. 1992, ApJ, 387, 95

Jarvis, M. J. & McLure, R. J. 2006, MNRAS, 369, 182

Kaspi, S., Smith, P. S., Netzer, H., Maoz, D., Jannuzi, B. T., & Giveon, U. 2000, ApJ, 533, 631

Kaspi, S., Maoz, D., Netzer, H., Peterson, B. M., Vestergaard, M., & Jannuzi, B. T. 2005, ApJ, 629, 61

Labita, M., Treves, A., Falomo, R., & Uslenghi, M. 2006, MNRAS, 373, 551

La Mura, G., Popović, L. Č., Ciroi, S., Rafanelli, P., & Ilić, D. 2007, ApJ, 671, 104

La Mura, G., Di Mille, F., Ciroi, S., Popović, L. Č., & Rafanelli, P. 2009, ApJ, 693, 1437

McLure, R. J. & Dunlop, J. S. 2002, MNRAS, 331, 795

Netzer, H. 1990 in Active Galactic Nuclei, ed. R. D. Blandford, H. Netzer, & L. Woltjer (Berlin: Springer) 137

Nikołajuk, M., Czerny, B., & Ziólkowsky, J. 2005 in AIP Conf. Proc. 801, Astrophysical Sources of High Energy Particles and Radiation, ed. T. Bulik, B. Rudak, & G. Madejski (Melville: AIP), 220

Onken, A. C., Ferrarese, L., Merritt, D., Peterson, B. M., Pogge, R. W., Vestergaard, M., & Wandel, A. 2004, ApJ, 615, 645

Osterbrock, D. E. 1989, Astrophysics of Gaseous Nebulae and Active Galactic Nuclei (1st ed.; Sausalito: University Science Books)

Peterson, B. M. & Wandel, A. 1999, ApJ, 521, 95

Popović, L. Č. 2003, ApJ, 599, 140

Popović, L. Č. 2006, ApJ, 650, 1217 (an Erratum)

Popović, L. Č., Mediavilla, E., Bon, E., & Ilić, D. 2004, A&A, 423, 909

Statler, T. S. 1995, AJ, 109, 1371

Sulentic, J. W., Marziani, P., & Dultzin-Hacyan, D. 2000, ARA&A, 38, 521

Sulentic, J. W., Repetto, P., Stirpe, G. M., Marziani, P., Dultzin-Hacyan, D., Calvani, M. 2006, A&A, 456, 929

Tonry, J. & Davis, M. 1979, AJ, 84, 1511

Van Der Marel, R. & Franx, M. 1993, ApJ, 407, 525

Vestergaard, M., Wilkes, B. J., & Barthel, P. D. 2000, ApJL, 538, 103

Woo, J.-H & Urry, C. M. 2002, ApJ, 579, 530